PAPER NO. 87-2624

PREFERENTIAL SOLUTE TRANSPORT THROUGH LAYERED SOILS

By

G.H. Oosting
Research Specialist

R.J. Glass
Research Assistant

T.S. Steenhuis
Associate Professor

Department of Agricultural Engineering
Cornell University
Ithaca N.Y. 14853, U.S.A.

For presentation at the 1987 Winter Meeting
AMERICAN SOCIETY OF AGRICULTURAL ENGINEERS

Hyatt Regency Hotel
Chicago, Illinois
December 15-18, 1987

SUMMARY:

Laboratory solute transport experiments were carried out in sandy soils where a fine textured layer overlies a coarse layer. Pulses of blue dye were used to characterize the solute movement. Unlike piston flow the solute moved in preferred path or "fingers" induced by infiltration flow instability. Shapes of the break-through curves were surprisingly similar to those observed in columns with homogeneous flow. Implications for solute sampling in the vadose zone are discussed.

American Society of Agricultural Engineers

St. Joseph, MI 49085-9659

PREFERENTIAL SOLUTE TRANSPORT THROUGH LAYERED SANDS

G.H. Oosting, R.J. Glass and T.S. Steenhuis

INTRODUCTION

Over the past twenty to thirty years the application of solute transport theory based on laboratory soil column experiments to field situations has been less than successful. There is a growing realization that the piston type flow observed in laboratory columns (Bodman and Coleman, 1943) does not adequately describe field solute transport. This should not be surprising as more than a century ago, Lawes et. al. (1882) found that a large proportion of water added to a soil only slightly interacted with that already present in the root zone. Yet, the piston flow model still forms the basis of conventional models currently in use (Carsel et al., 1985, Leonard et al., 1985, Nofzinger and Hornsby, 1986, Steenhuis and Naylor, 1987 Jury et al, 1987).

At present, research on nonpiston type heterogeneous flow can be divided into two approaches: statistical and phenomenological. The statistical approach superimposes on the piston flow model a distribution of solute travel times obtained from intensive random sampling of an individual field. This approach will yield a good prediction of the transport of pollutants to the water table under a particular field but intensive sampling must be done for each field in question, a time consuming and expensive undertaking.

The phenomenological approach consists of defining and describing mechanisms that cause heterogeneous flow. Two mechanisms have been determined, that involving movement in isolated channels of high hydraulic conductivity or macropores (eg., Beven and Germann, 1982; Smettem and Collis-George, 1985; Richard and Steenhuis, 1987) and that due to wetting front instability also termed infiltration flow instability or "fingering".

Current field and laboratory evidence (Starr et al., 1987; van Ommen et al., 1987; and Glass et al., 1987) has shown that for soils whose hydraulic conductivity increases with depth but does not vary from point to point horizontally, wetting front instability can cause nonuniform solute transport. In these soils, water and toxics can move in preferred paths to groundwater at speeds approaching the saturated hydraulic conductivity of the subsoil.

In this paper, we present the results of experiments designed to study the effect of the wetting front instability that occurs when a fine textured layer overlays a coarser bottom layer on solute transport through the layered system.

EXPERIMENTAL METHOD

A two-dimensional unstable flow field was generated in a plexiglass chamber 1 cm deep, 51 cm wide and 140 cm high. The chamber was filled with two layers of sand with the top layer much finer than the bottom layer. On one side of the chamber about 100 holes allowed air to escape freely. The holes were small

enough to prevent sand from escaping but large enough that water never entered them during an experiment. White silica sand, used commercially for sand blasting, was sieved through US sieve series numbers 14, 40 and 200. The 14-40 fraction was used for the coarse bottom layer while that which passed the 200 sieve constituted the top fine layer. The sands were cleaned and dried before and between uses to assure purity. The chamber was filled with the bottom sand layer through a funnel/extension/randomizer assembly to minimize segregation and heterogeneities and then packed using a drop impact method. After packing, at least 10 cm of the top of the coarse sand layer was removed to bring the bottom layer thickness to 129 cm. After making the textural interface as flat as possible, the fine top layer was added and tamped a centimeter at a time until it was 8 cm thick. Sand cleaning and chamber filling and packing procedures were described in detail in Glass et al., (1987).

The initial moisture distribution was varied systematically by running four consecutive infiltration experiments. In the first experiment, denoted by a capital "A" following the experiment number, the sand was initially air dry. A depth of 1.5 cm of water was ponded and maintained for 72 hours during which solute pulses were added at 4, 24 and 48 hours. The chamber was then sealed at the top to inhibit evaporation and allowed to drain by gravity for twenty-four hours. The moisture content field at the end of the drainage cycle formed the initial moisture field for the second experiment.

The second experiment, denoted by a capital "B" following the experiment number, was then conducted with a steady ponding level of 1.5 cm for 72 hours again with solute pulses at 4, 24 and 48 hours. After 24 hours of drainage of this "B" experiment, 1.5 cm of water was added every 8 hours for a two week period with the first 1.5 cm containing the solute. This experiment simulating intermittent irrigation events we denote by "Bint" following the experiment number.

In preparation for the fourth and final experiment, the bottom layer was saturated several times, sealed and drained for another twenty-four hours. A uniform moisture content of 6% in the bottom layer resulted. This final experiment was also conducted with a steady ponding level of 1.5 cm for 72 hours with solute pulses at 4, 24 and 48 hours and is further denoted by a capital "C" following the experiment number. In this way the first ("A") and fourth ("C") experiments represented the initial moisture content conditions (i.e uniform) often used in analytical and numerical studies of infiltration flows. The second and third experiments mimic more realistically field situations where initial moisture content varies from point to point, and infiltration is either steady ("B") or intermittent ("B_{int}").

Distilled water with a constant low non-adsorbing dye concentration (.025 % solution of USDA Red #3) was used in all of the experiments. The red dye made the flow field visible. Pulses of USDA blue #1 dye solution (approximately 0.058 %) were used for characterization of the solute transport. Pulses were added to the A, B and C experiments by allowing the ponding level to decrease to 1 cm after which 25.5 ml of a known concentration of blue dyed water was mixed thoroughly in the ponded water. Constant ponding to a level of 1.5 cm was resumed just as all blue dyed water had moved into the top layer. In addition to being able to measure the concentration of the blue dye out the

bottom of the chamber, the movement of the solute through the chamber was easily visualized and documented with time lapse photography on movie film. Data was pulled from the film by projecting it onto a screen and then tracing the wetting front position with time on acetate sheets.

To measure the flow variability of both water and solute, the flow out the bottom of the chamber was measured through 17 separate sections each having a width of 3 cm. These "drip sections" restricted the lateral movement of water at the bottom of the chamber and thus enabled the monitoring of the flux of both water and solute through individual fingers and its change in time.

Water was collected from each drip section in time and the concentration of the blue dye in each sample was measured using the colorimetric method. A photo-spectrometer was used at a wavelength of 685 mm and a standard curve, relating transmittance to concentration, was determined at the time of each pulse through a series of standard solutions of known concentration.

A smaller subset of the experiments described was conducted first followed by the complete set. We will refer to these two sets as experimental sets numbers 1 and 2 respectively. Table 1 presents a summary of all the experiments conducted.

TABLE 1: EXPERIMENTS CONDUCTED

Experiment run number	Initial moisture condition	Begin time of pulse (hours)	Flow rate (ml/min)	t_{peak} (*) (min)
1A1	dry	4	21.74	24.5
1A2		24	20.88	25.5
1B1	1 day after 1A	4	19.98	54.0
1B2		24	16.98	62.0
$1B_{int}$	1 day after 1B	0	0.14	3420
2A1	dry	4	21.35	25.5
2A2		24	20.97	25.5
2A3		48	20.05	25.5
2B1	1 day after 2A	4	20.05	41.0
2B2		24	20.74	43.0
2B3		48	19.63	47.0
$2B_{int}$	1 day after 2B	0	0.14	3120
2C1	1 day after $2B_{int}$	4	20.00	60.5
2C2		24	18.66	65.5
2C3		48	19.22	60.5

(*) Peak time of concentration

FIGURE 1

FINGER / FRINGE DEVELOPMENT EXPERIMENT 1

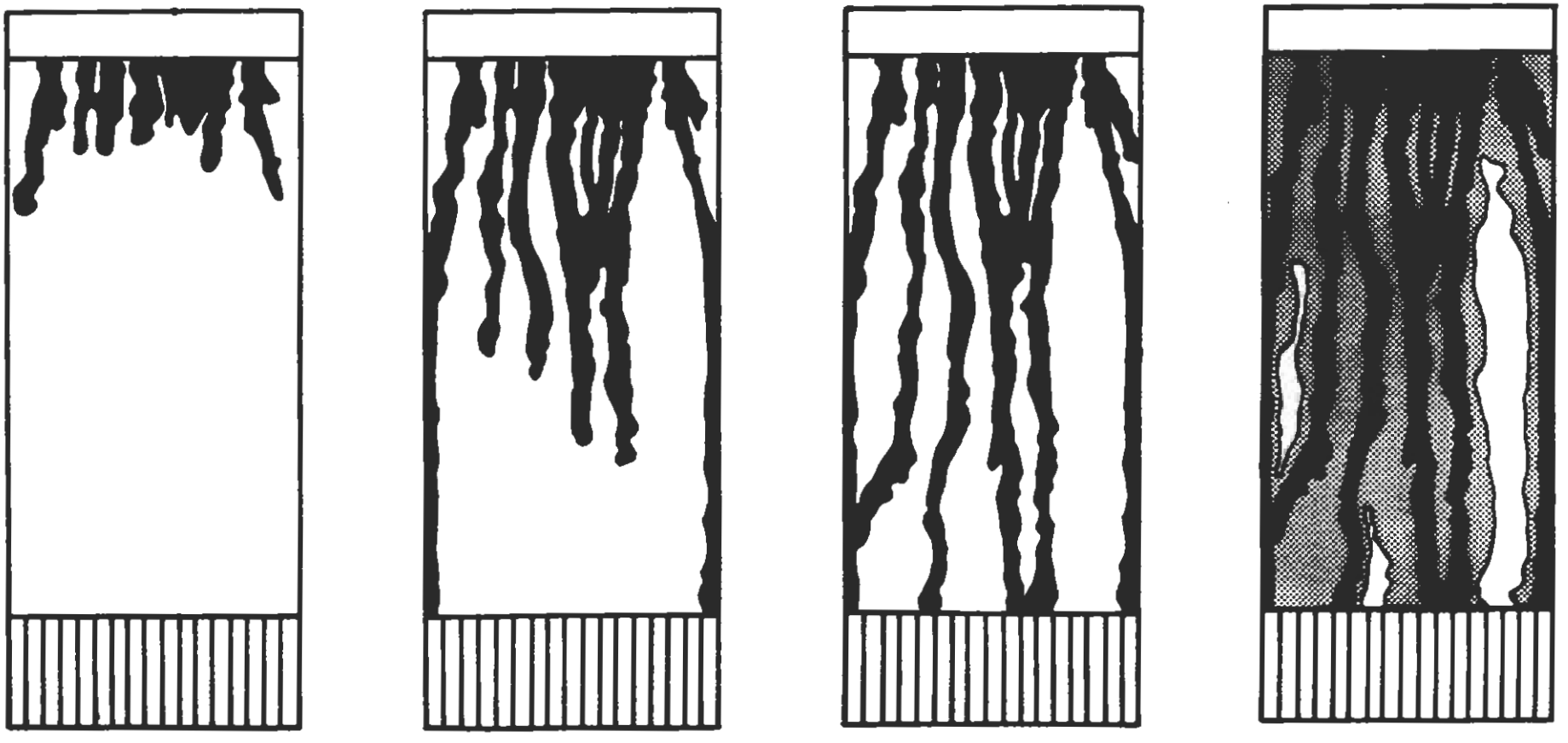

a) 7 min

b) 15 min

c) 30 min

d) 4 hrs

51 cm

RESULTS

Results of our experiments will be divided into two sections, flow field structure and solute breakthrough curves. The structure of the flow field is of great consequence for solute transport and so a detailed discription of that structure will be given.

Flow field Structure

In all experiments wetting front movement within the top fine layer was stable while instabilities occured in the bottom coarse layer. In the "A" experiment, water crossed into the coarse layer at many discrete points each generating a small finger many of which then merged to form larger faster moving fingers which continued to move downward. While these fingers continued to conduct most of the flow through the chamber, slow sideways moving wetting fronts passed from these finger core areas into the dry sand on either side of the finger creating a surrounding fringe area. These fringe areas are at a much lower moisture content than the finger core areas which continue to conduct most of the flow. Figure 1 is a drawing of finger development in the bottom layer of experiment 1A showing the rapid downward growth followed by a stage of slow lateral growth into the fringe areas.

Once the laterally moving wetting fronts had passed through all of the dry sand, very little change in flow field could be detected. The dramatic fringe and core region structure within the bottom coarse layer persisted for the duration of the 72 hour infiltration cycle.

Table 2 presents the number of final fingers, average width, average finger tip velocity and % total area of the chamber occupied by fingers for experiments 1A and 2A. This data can be used to represent the structure of the flow field and shows this structure to be very similar between the two experimental sets.

TABLE 2: FINGER PROPERTIES

Experimental set	Final # of fingers	Average width +/-STD (cm)	% of chamber occupied by fingers	Average velocity +/-STD (cm/min)
1	6	2.14+/-0.50	25.2	6.51+/-2.05
2	6	1.59+/-0.21	18.7	7.06+/-1.75

At the start of the B experiment 24 hours after the water flow in the A experiment was stopped, the initial moisture content field appeared almost uniform to the eye. However, upon ponding in the B experiment, the fringe and core structure in the bottom layer again reappeared. The locations of the core regions as highlighted by the blue pulses were almost the same in the B experiment as those in the "A" experiment.

FIGURE 2

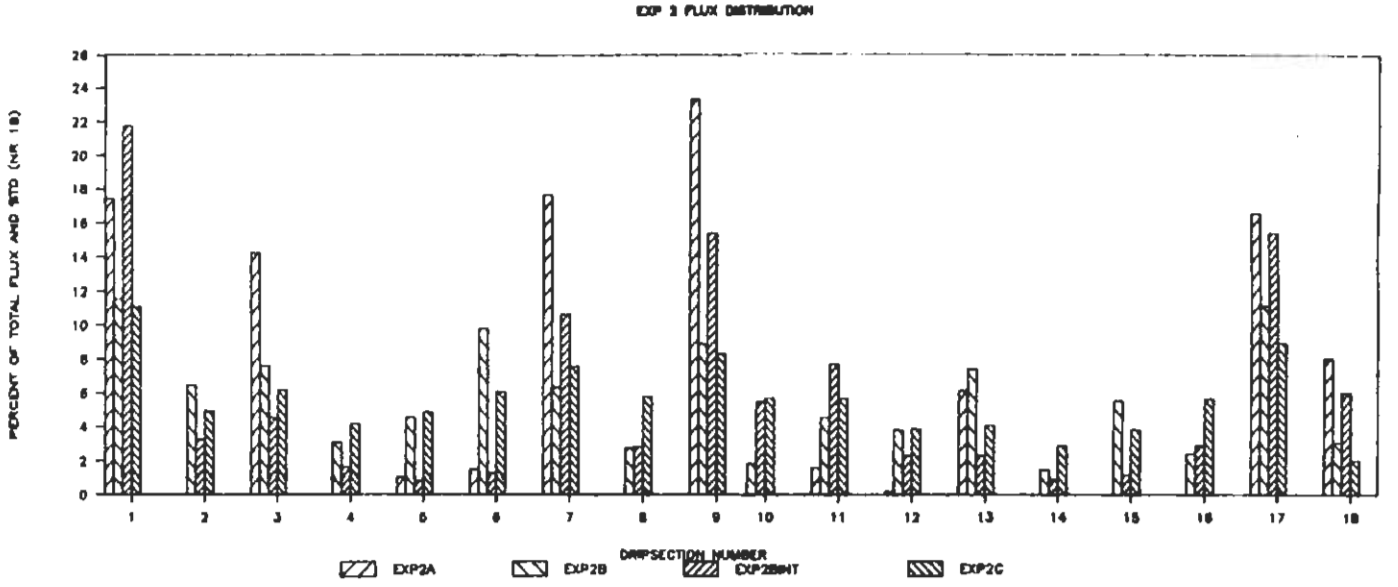

FIGURE 3

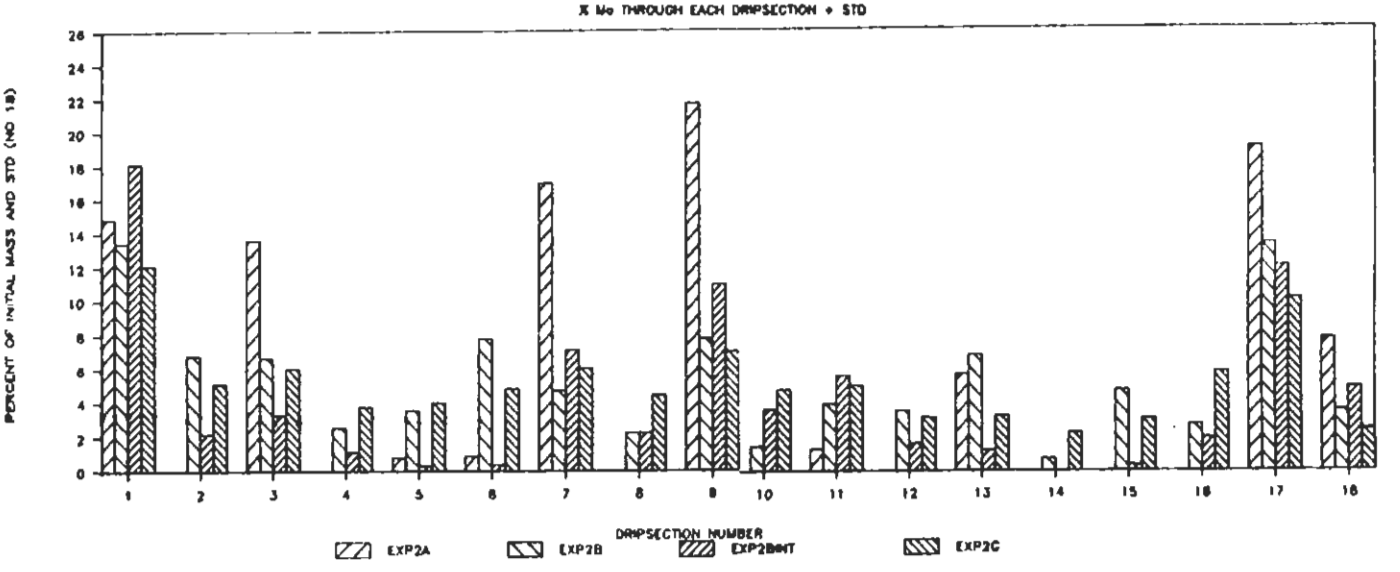

In general the participation of the fringe areas in conducting water and solute has increased over the "A" experiment, however the core regions continue to conduct the majority of the flow. This persistence of core and fringe structure has been documented by us for at least 4 infiltration cycles such as this one, the final one with steady infiltration for 10 days.

In the "B_{int}" experiments when water was applied intermittently, the finger structure in the 30 cm directly below the textural interface was the same as in the ponded A and B experiments. Below this region the structure became more complicated and there was more merger of fingers. Essentially three regions, one on each side and one in the middle, conducted the majority of the water and dye. The sizes of the regions were about 9, 6 and 20 cm respectively.

In the final "C" experiment the moisture content was initial uniform. As the wetting front moved from the textural interface it became wavy, the amplitude of the wave increasing in depth. Such an increase in amplitude with depth is a definition of instability, however, the dramatic finger structure found in the A, B and B_{int} experiments was not present. Blue dye pulses showed an exaggeration of the wave form of the initial wetting front with wide diffuse core areas in the middle and along each side of the chamber. This flow field structure illuminated by the blue pulses changed little over the 72 hour infiltration period.

Both the flux and the total solute mass distribution over the 17 drip sections at the bottom of the chamber for each of the A, B, B_{int} and C experiments can be used to show the extreme deviation from the homogeneous flow usually assumed for our experimental situation. Figure 2 presents the percent of the total flow for each drip section in the experimental set 2 and figure 3 the percent total mass transported through each drip section. As expected there is close agreement between the percent flow and the percent mass carried by a particular drip section. The standard deviation across the 17 drip sections can be used as a measure of the uniformity of the flow field: the more uniform, the lower the standard deviation. The standard deviation is plotted in figures 2 and 3 in the last column (no. 18). It is seen to decrease from the A to the B to the C experiment from 8.0 to 3.3 to 2.1 for the flow ditribution and from 7.8 to 3.6 to 2.5 for the % mass distribution. However, in experiment B_{int} the standard deviation essentially doubled from its value in the B experiment from 3.3 to 6.1 for the flow distribution and from 3.6 to 4.9 for the % mass distribution.

Breakthrough Curves

Total chamber breakthrough curves (BTC) showing the relative concentration, C/C_o in time where C is the concentration of the fluid exiting the bottom of the chamber and C_o is the initial concentration can be constructed from the data obtained from the individual drip sections over time. Figure 4 combines the BTC's for all pulses of the A, B, and C experiments of experimental set 2. All of the pulses for each experimental set had a slightly different initial concentrations, C_o, initial mass, Mo, and total volumetric flow rates, Q. Thus, in order to compare the BTC's we plot the solute flux verses time in non-dimensional form. The non-dimensional solute or mass flux, M^*, is defined as

FIGURE 4

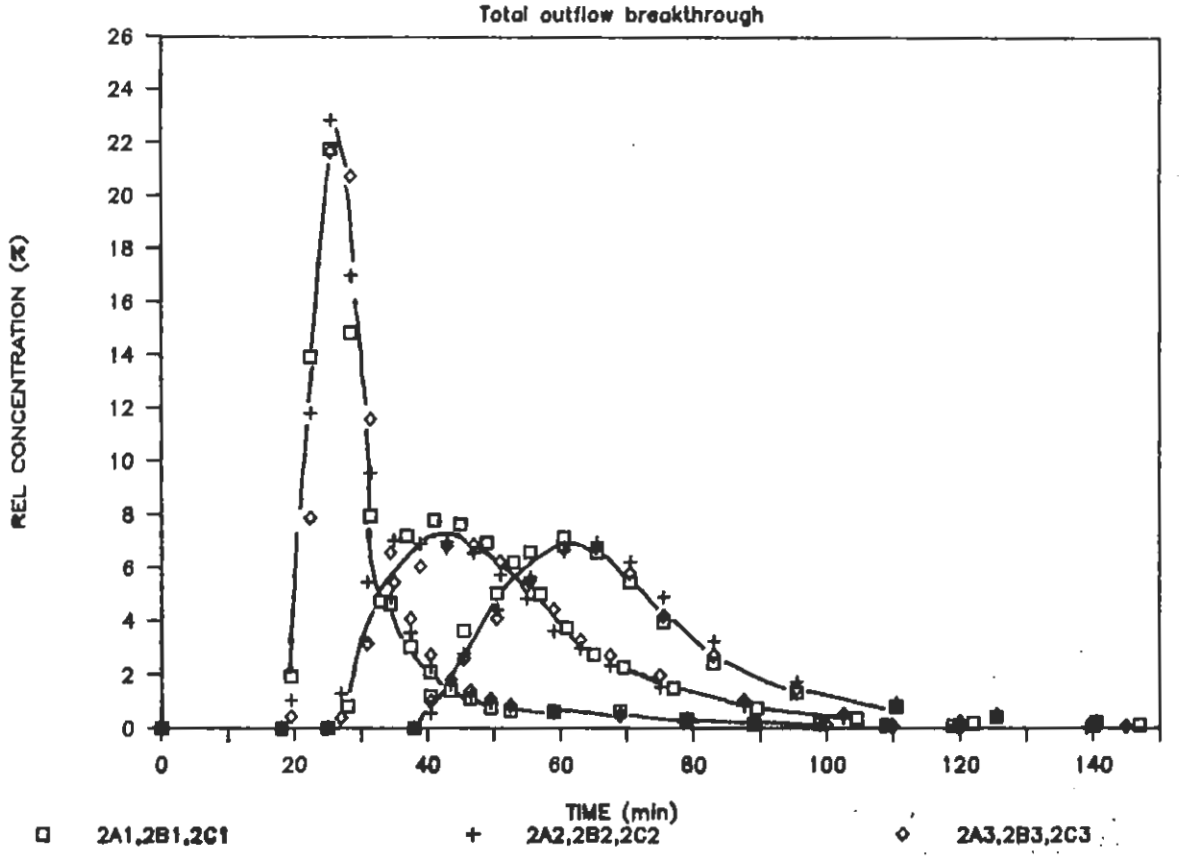

FIGURE 5

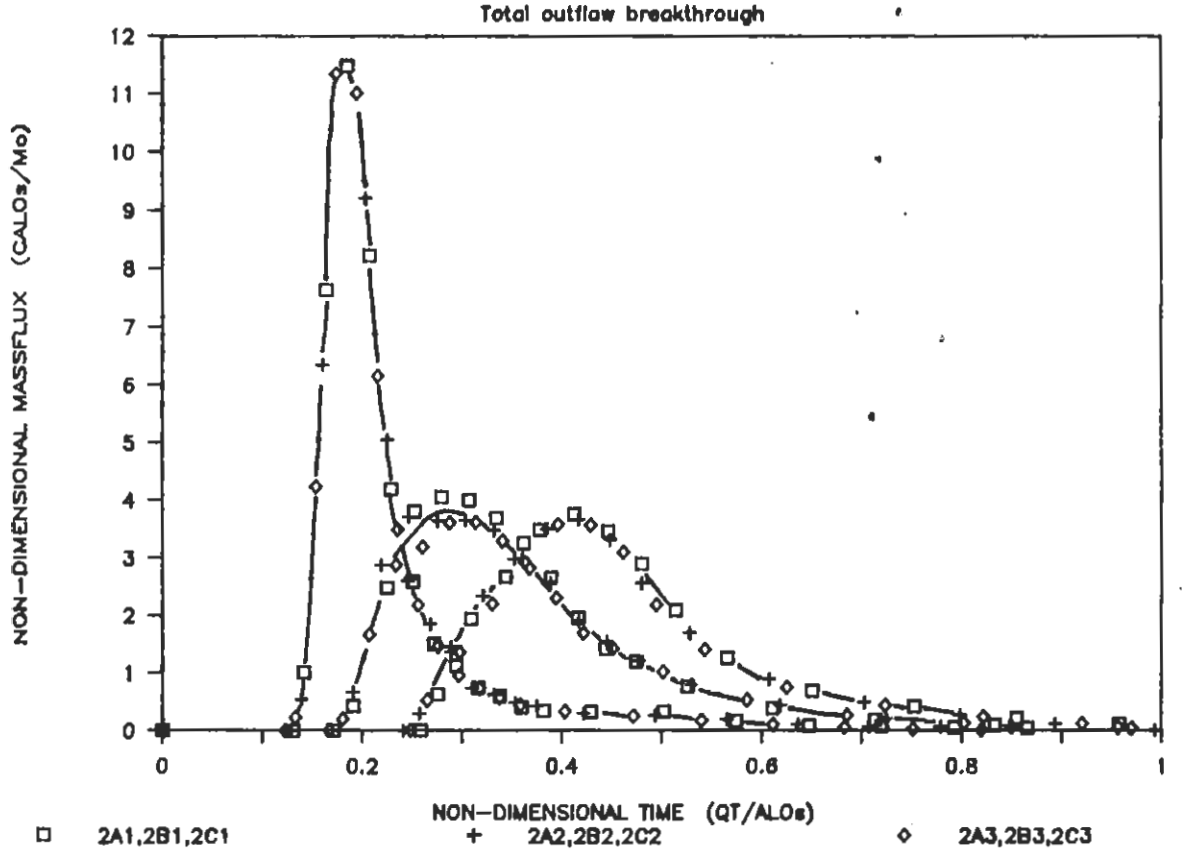

$$M^* = C\ A\ L\ f\ /\ M_o$$

where A is the cross sectional area of the chamber, M_o is the initial mass of solute applied, L is the total length from the top of the upper layer to the bottom of the lower layer, and f is the porosity of the bottom layer. The non-dimensional time is given as

$$t^* = Q\ t\ /\ A\ L\ f$$

where Q is the total flow rate through the chamber. In this non-dimensionalization we use f rather than the traditional choice of the moisture content within the chamber. Choise of this moisture content would equate non-dimensional time to pore volume. In our case θ varies substantially in the horizontal for the core-fringe structured flow field. Use of f provides a proper non-dimensionalization and allows comparison of all pulses. A value of one for t^* can be considered as one pore volume when the chamber is entirely saturated, or $\theta_s = f$.

Breakthrough curves in M^* and t^* for all pulses in the A, B, and C experiments for the second experimental set are shown in figure 5. A line is drawn by hand through the data to distinguish the three experiments better. As can be seen from figure 5 the three breaktrough curves within each of the A, B and C experiments are almost identical and show no trend in time over the 72 hour infiltration event. This therefore supports the visual impression that very little change in flow field structure occurred once the initial wetting fronts had moved through the chamber. In addition, reproducibility confirms that our experimental techniques were consistent and not responsible for the changes in shape and position of the breakthrough curve as we progressed from the A to the C experiments.

The peak time and height increases and decreases respectively from the A through the C experiment. The very small effect of the fringe area in conducting water and solute in the A experiment is further emphasized by the fact that at the time of the first pulse, the lateral wetting fronts had yet to wet the entire chamber.

Figure 6 shows a comparison between experimental sets of the first pulses in the A and the B experiments. Since the initial flow field is unstable and its structure persists into the B experiments their breakthrough curves would not be expected to be completely similar. However, figure 6 shows them to be remarkably similar especially for the A experiment. This indicates that chamber scale structure of the flow field caused by the initial instability in a particular situation may be reproduced without duplicating the individual fingers, their exact paths and interactions.

The BTC's of the two intermittant experiments ($1B_{int}$ and $2B_{int}$) are shown in figure 7. Again we see remarkable correspondence between the two. Comparison with figure 5 shows the peak for the intermittent experiment to come through before that of the A experiment. The Bint experiments were stopped after 70% of the total mass had moved through the chamber since the tail on the BTC was very long and our experimental time was restrictive. The final 30% of

FIGURE 6

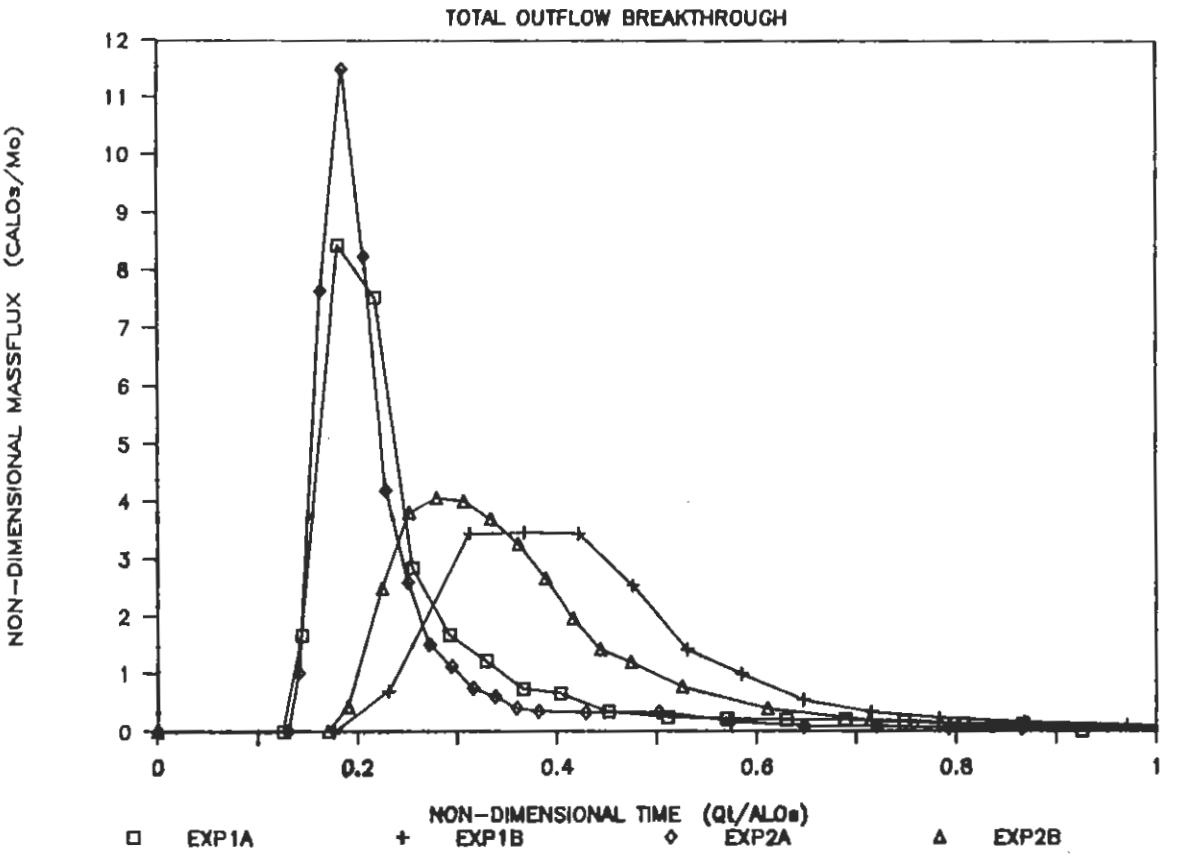

FIGURE 7

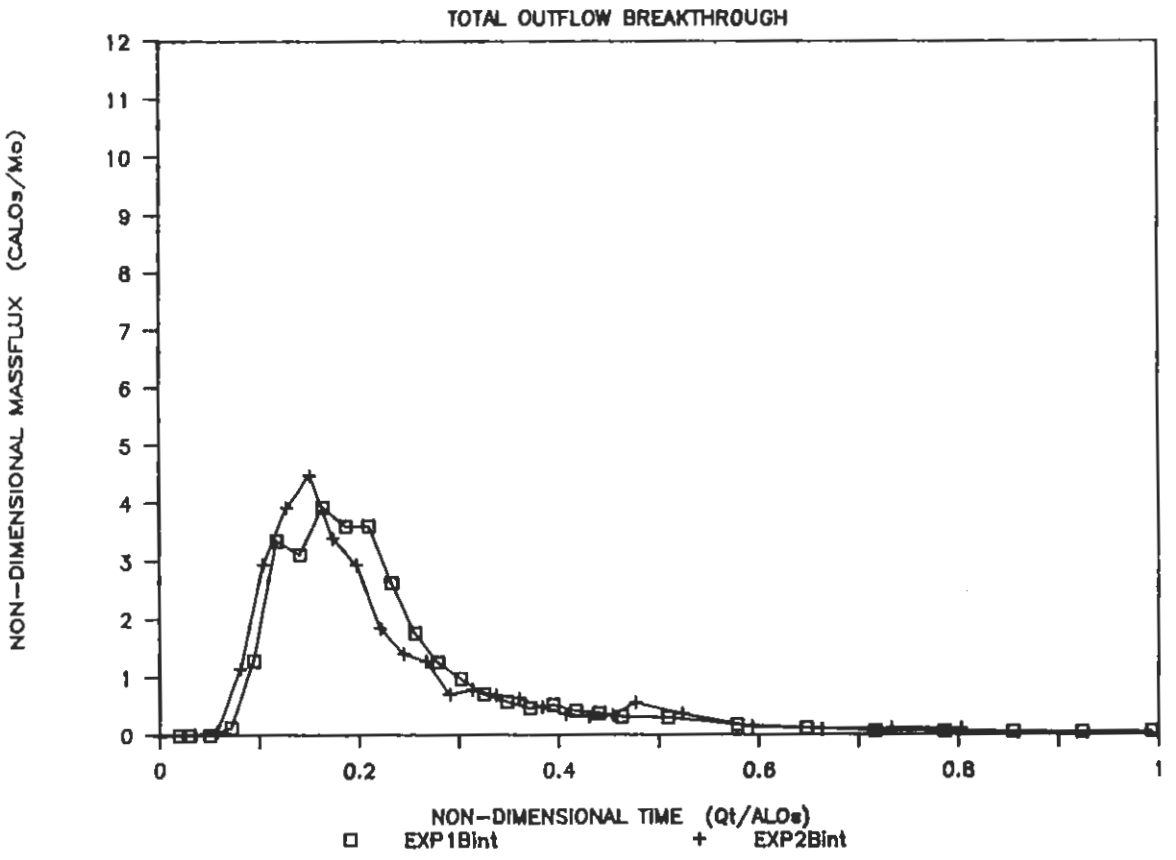

FIGURE 8

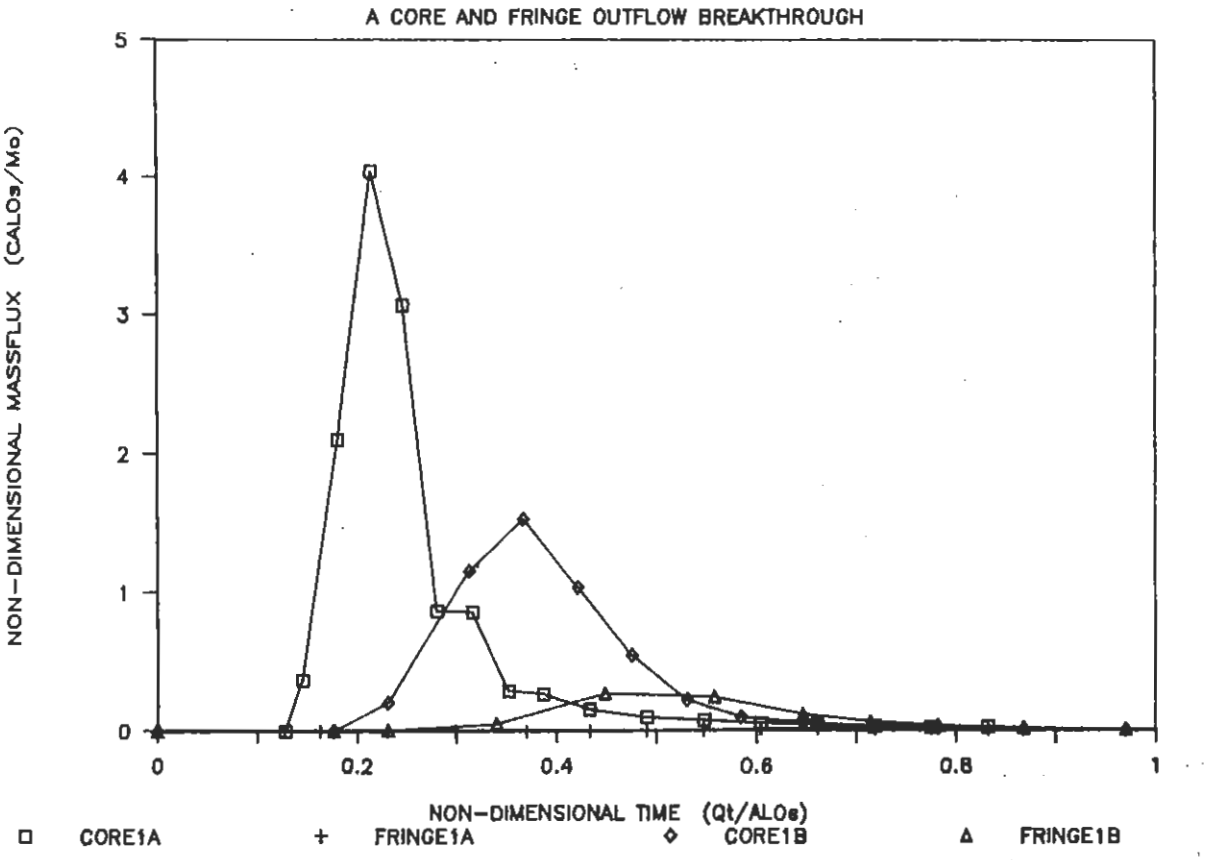

FIGURE 9

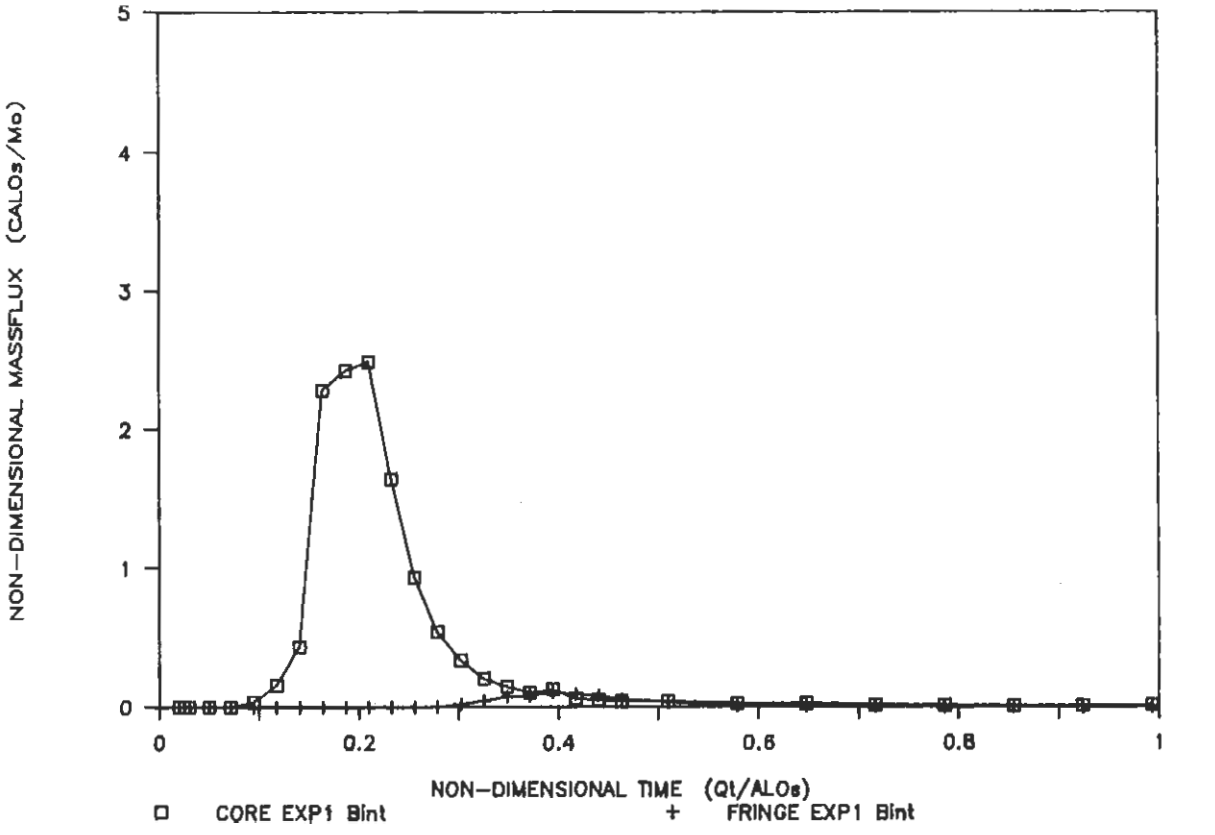

the mass would continue "trickle" out at a very low concentration over a very long length of time.

The monitoring of water and mass flux out of the individual drip sections gives the opportunity to compare the contribution of the core and fringe structural regions. Figures 8 through 9 compare a core area with an adjoining fringe area. These two regions were selected because their flows would be easily seperated. Figure 8 and 9 show the response of the core and fringe for the first pulses of the A and B experiments and the B_{int} experiment respectively. In the A experiment the contribution of the fringe area with its peak t^* .7 is almost undetectable on the plot. For the B experiment the core area M^* decreases, its distribution in t^* spreads out and the peak t^* shifts to the right. Alternatively, the B fringe areas peak M^* increases, and its peak t^* shifts to the left. Thus, for the B experiments, the core and fringe area response remains seperate but has shifted closer together. The B_{int} experiment reverses this trend with the peak separating further in both t^* and M^*.

COMPARISON WITH ANALYTICAL SOLUTION ASSUMING HOMOGENEOUS FLOW

In the first stage of analysis of the rather complicated mixing processes acting within the bottom layer we will analyze the BTC as if we knew nothing of the structure within the bottom layer and treat the flow fields as if it was homogeneous. For simplicity we choose the most rudimentary analytic solution to the one dimensional advective dispersion equation that would approximate our situation. If we assume that the solute is applied in a band of infinitesimal thickness at the textural interface between the upper and lower layers, that above the textural interface the coarse sand extended upward indefinitely instead of the fine layer, and that the bottom boundary has no effect on water or solute movement then we have

$$C = \frac{M_o}{A\,\theta\,(4\,\pi\,D\,t)^{\frac{1}{2}}}\,\exp\left(\frac{-\,(L - v\,t)^2}{4\,D\,t}\right) \qquad (1)$$

where D is the dispersion coefficient, L is the length of the coarse layer, v is the average pore velocity given by L/tp, and θ is the effective moisture content within the bottom layer. We may rewrite equation (1) in terms of M^* and t^*

$$M^* = \frac{A\,L\,f\,v}{(4\,\pi\,D\,Q\,L\,f\,t^*)^{\frac{1}{2}}}\,\exp\left|\frac{-\,(L - v\,\frac{A\,L\,f}{Q}\,t^*)^2}{4\,D\,\frac{A\,L\,f}{Q}\,t^*}\right| \qquad (2)$$

using the definition $v = Q/A\theta$. To apply equation (2) we translate $t^* = 0$ to the point where the pulse band is half way across the textural interface. Equation

FIGURE 10

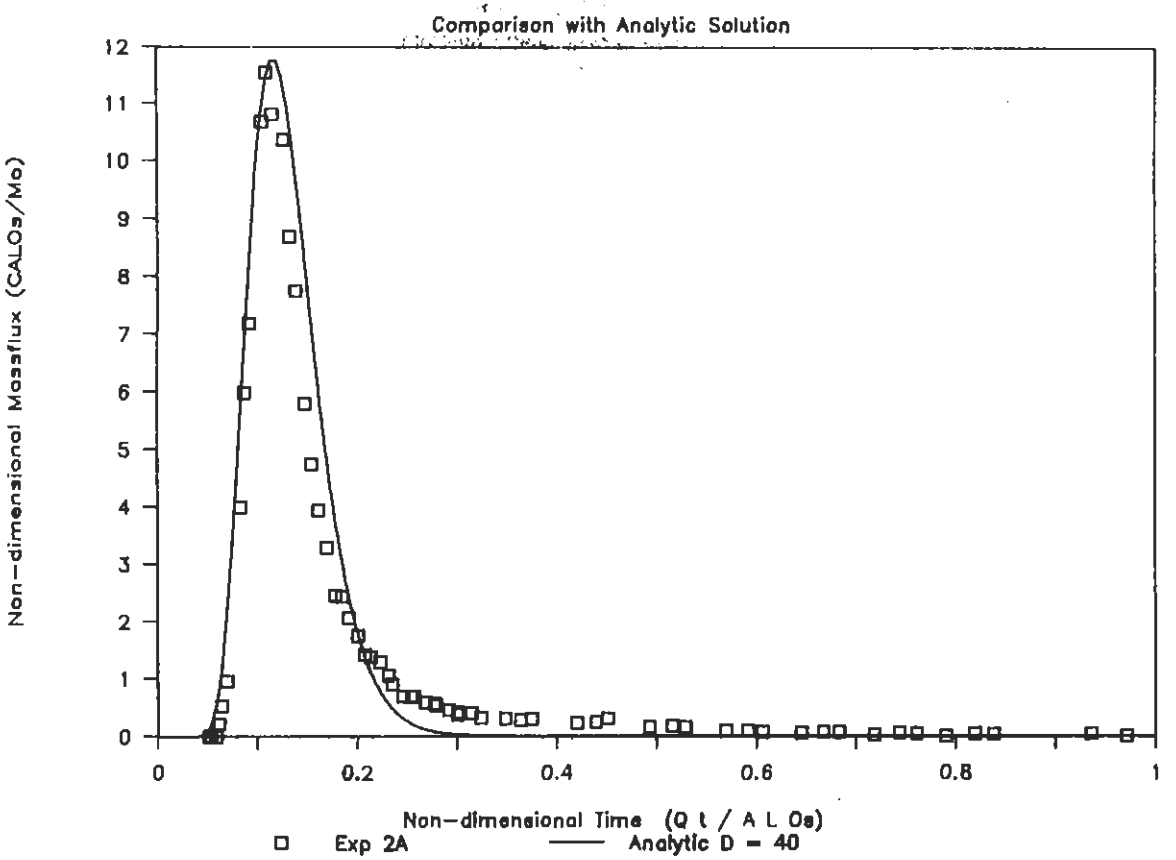

FIGURE 11

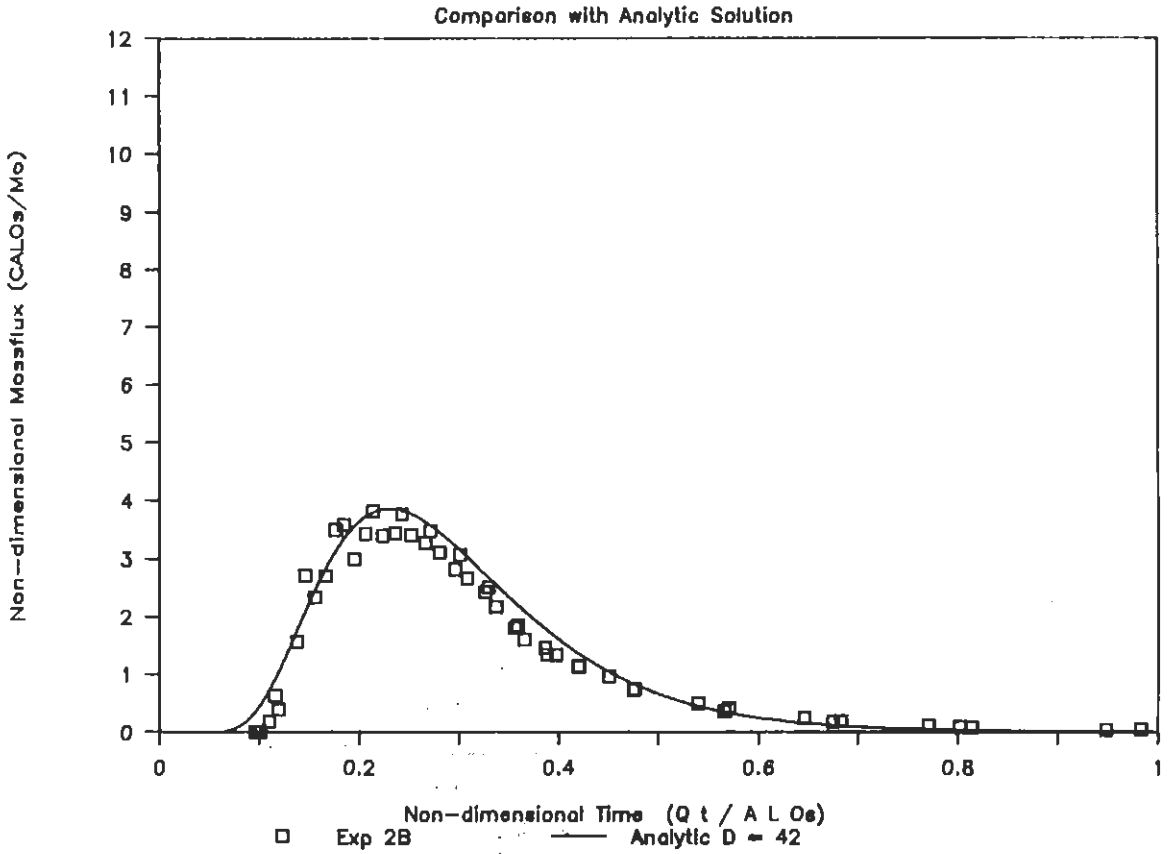

FIGURE 12

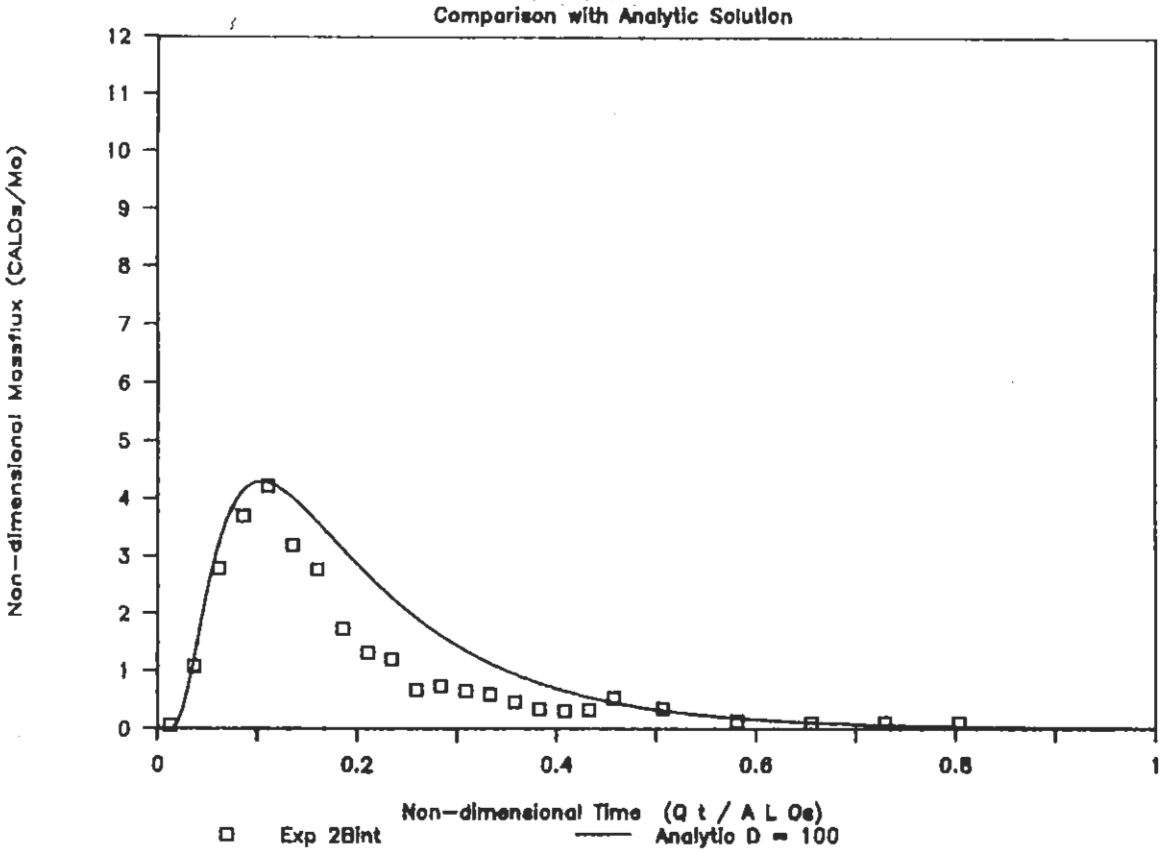

FIGURE 13

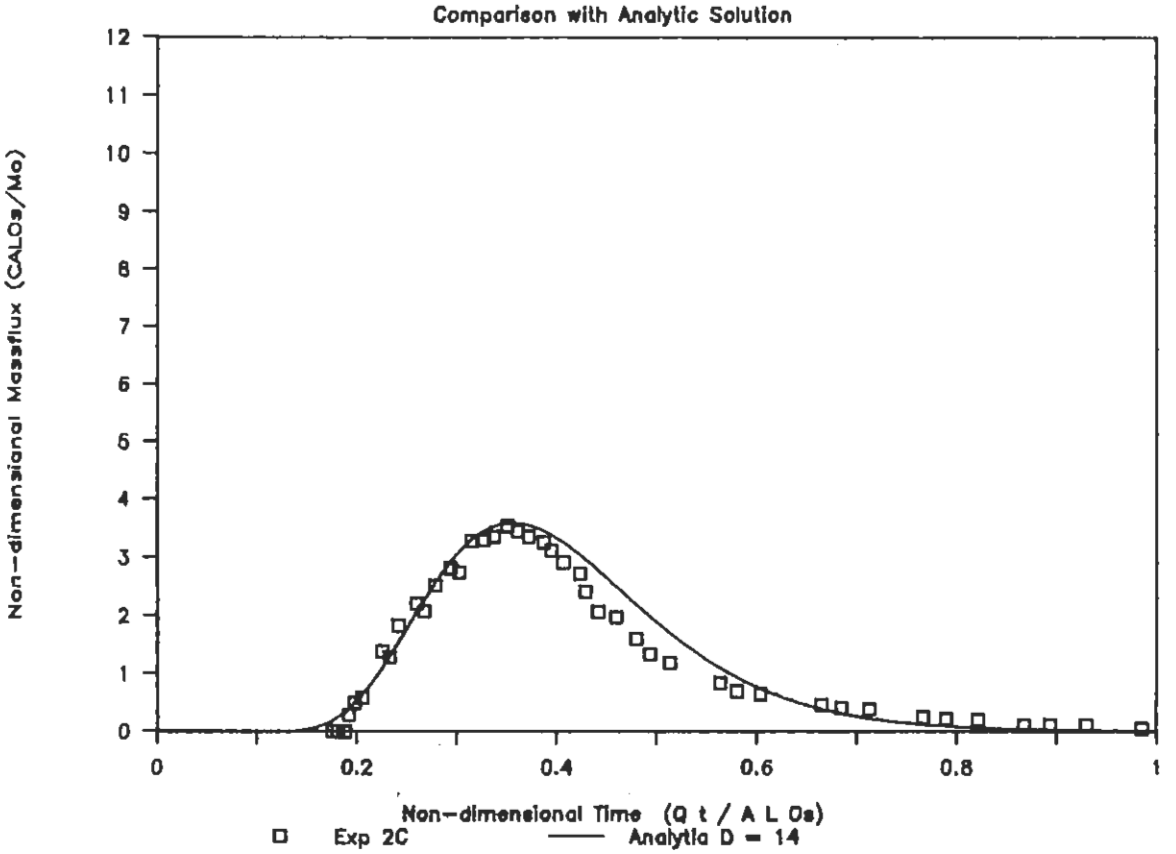

(2) was then graphically fitted to the pulse data for experimental set 2. The data for all pulses of a particular experiment are combined for the fit. The values of tp, v and the best fit D are given in Table 3.

TABLE 3: BTC PARAMETERS

Experiment #	Translated time to peak (min)	Q (ml/min)	v (cm/min)	D (cm2/min)
2a	16.3	20.79	7.94	40
2b	34.6	20.14	3.73	42
$2B_{int}$	2640	0.14	0.49	17
2C	55.5	19.29	2.41	14

Figures 10 through 13 show the data and equation (2) plotted for the values of v and D chosen. The fit of equation (2) to the data appears to be fairly close. Equation (2), however, does not fit the falling side of the break through curve, consistently first over predicting and then under predicting M^*. This error is seen most dramatically for the B_{int} experiment where 30% of the mass is yet to leave the column at $t^* = 1$ and would constitute an extremely long tail.

The fact that equation (2) can be used to "predict" the majority of the BTC is not too surprising as the form of the BTC ignoring the tail is very similar to the form of equation (2). The t^* of the peak is simply fit by the calculation v = L/tp and D is chosen to give the required spread. From this point of view, equation (2) is simply forced on the data and we are left with a dispersion coefficient. The dispersion coefficients in table 3 are not unlike those found in other experiments where no preferntial movement was documented, may be with exception of the B_{int} experiment. We are in the process of examining these data to test the usefulness of the mobile-immobile model for unstable flow fields.

IMPLICATIONS

Wetting front instability has important implications for both monitoring and predicting the fate of the toxics in the unsaturated zone. The usual practise in monitoring programs is to sample one or two locations. Consequently, if fingering is occuring then the sample might indicate a significantly higher or lower movement than the "average".

Figures 14 and 15 show the response of the same core and fringe areas as in figure 9 and 10 with the relative concentration C/Co plotted verses t*. If one monitored the solute in the field from a probe located within a fringe area

FIGURE 14

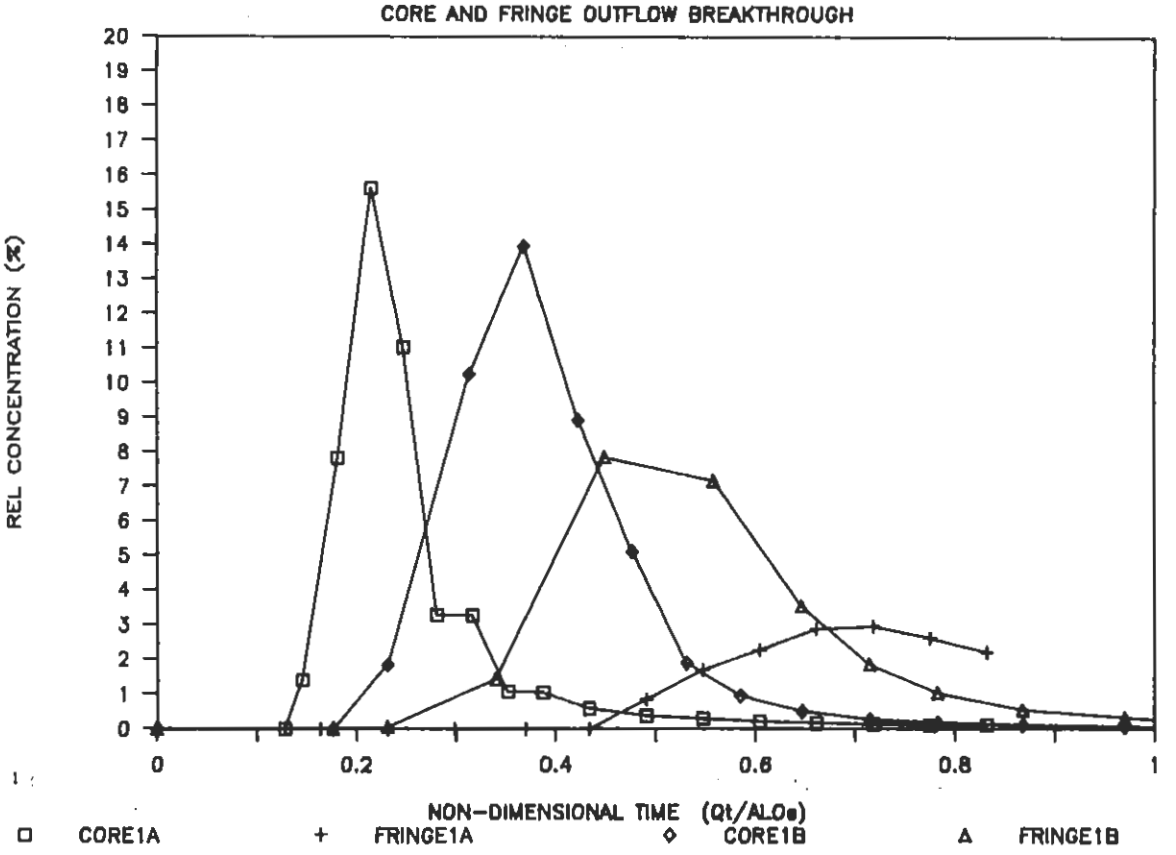

FIGURE 15

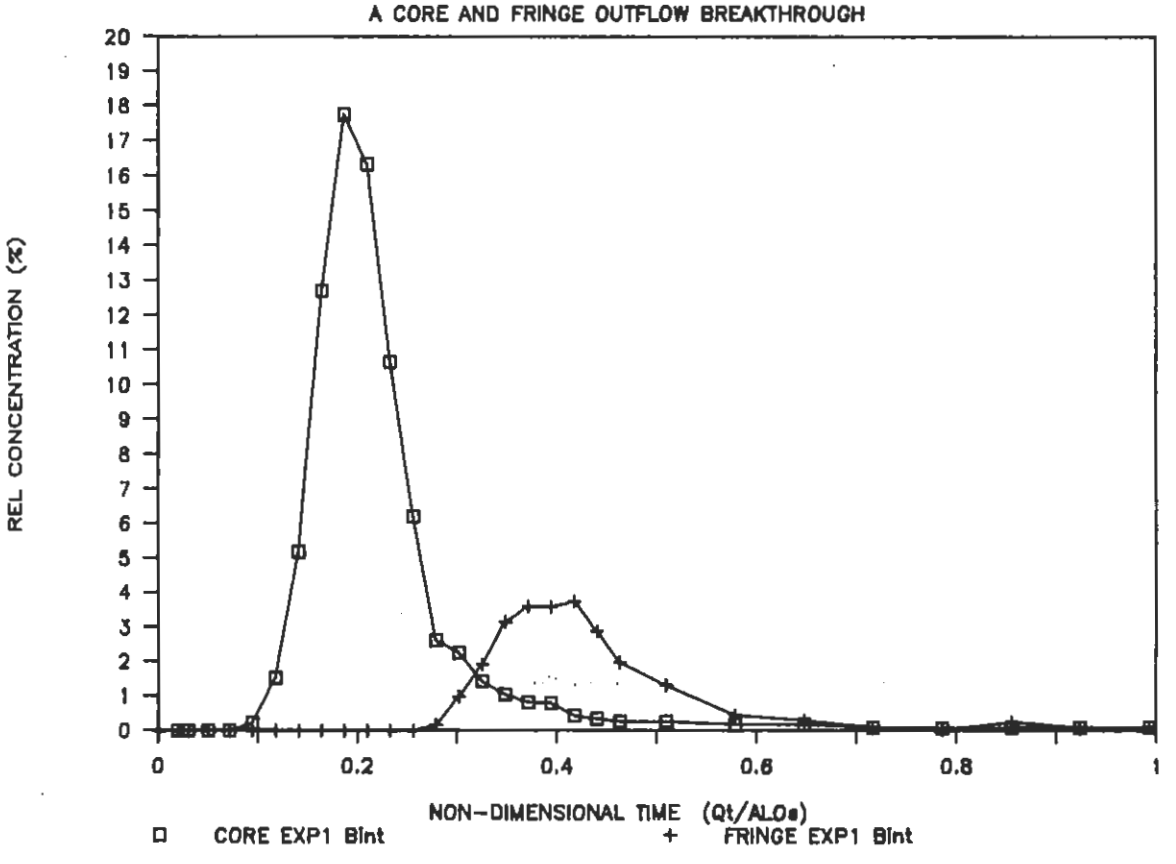

or a core area, this would be the usual way the data would be presented. Such data could lead to various miss interpretations, especially if no finger areas were sampled.

The figures 9 and 10 presents M* verses t* and properly weights the regions by their flow rate. The core regions dominate the fringe regions and emphasize the need for sampling techniques that integrate the flow over a large enough region to sample core areas. Such a technique is currently being studyied by N. Baily at Cornell University (personal communication) both in the laboratory and in the field. The technique involves the use of suction lysimeters placed in the capillary fringe region above the water table. This method shows promise since water flow in the capillary fringe region is still vertical and as was shown in the laboratory experiments presented in this paper, fingers will widen and coalesce under high uniform moisture content.

REFERENCES

Beven, K., and P. Germann. 1982. Macropores and water flow in soils. Water Resour. Res. 18:1311-1325.

Bodman, G.B. and E.A. Colman. 1943. Moisture and energy conditions during downward entry of water into soils. Soil Sci. Soc. Am. Proc. 8:116-122.

Carsel, R.F., L.A. Mulkey, M.N. Lorber, and L.B. Baskin. 1985. The pesticide rootzone model (PRZM): A procedure for evaluating pesticide leaching threats to groundwater. Ecological Modeling 30:49-69.

Glass, R.J., J-Y Parlange and T.S. Steenhuis. 1987. Water infiltration in layered soils where a fine textured layer overlays a coarse sand. Proceedings of the International Conference for Infiltration Development and Application, Hawaii, Jan. 5-9, 1987.

Jury, W.A., D.D. Focht, and Q.J. Farmer. 1987. Evaluation of pesticide groundwater pollution potential from standard indices of soil-chemical adsorption and biodegradation. J Environ. Qual. 16:422-428.

Lawes, J.B., J.H. Bilbert and R. Warington. 1882. On the amount and composition of the rain and drainage waters collected at Rothamsted. William Clowes and Sons, LTD. Londen.

Leonard, R.A., W.G. Knisel, and D.A. Still. 1986. GLEAMS: Groundwater loading effects of agricultural management systems. ASAE Paper No. 86-2511. American Society of Agricultural Engineers, St. Joseph, MI.

Nofziger, D.L., and A.G. Hornsby. 1986. A microcomputer-based management tool for chemical movement in soil. Applied Agricultural Research 1:50-56.

Ommen, van H.C., L.W. Dekker, R. Dejksma, J. Hulshof and W.H. van der Molen. 1987. A new technique for evaluation the presence of preferential flow paths in non-structured soils. SSSAJ in press.

Richard, T. and T.S. Steenhuis. 1987. Tile drain sampling of perferential flow on a field scale. Accepted for publication by Journal of Contaminant Hydrology.

Smettem, K.R.J. and N. Collis-George. 1985. Statistical characterization of soil biopores using a soil peel method. Geoderma 36:27-36.

Starr, J.L., J.Y. Parlange and C.R. Frink. 1986. Water and chloride movement through a layered field soil. Soil Sci. Soc. Am. 50:1384-1390.

Steenhuis, T.S., and L.M. Naylor. 1987. A screening method for preliminary assessment of risk to groundwater from land-applied chemicals. J. Contam. Hydrol., 1: 395-406.